Radiation Physics and Chemistry 237 (2025) 113032

Contents lists available at ScienceDirect

Radiation Physics and Chemistry

journal homepage: www.elsevier.com/locate/radphyschem

Thermoluminescence and optically stimulated luminescence of $CaSO_4$:Mn, Tb with different dopant concentrations

A.M.B. Silva [a,*], D.N. Souza [b], L.V.E. Caldas [a]

[a] Instituto de Pesquisas Energéticas e Nucleares, Comissão Nacional de Energia Nuclear, IPEN/CNEN-SP, Av. Prof. Lineu Prestes, 2242, 05508-000, São Paulo, SP, Brazil

[b] Departamento de Física, Universidade Federal de Sergipe, Av. Marechal Rondon, S/N, 49.100-000, São Cristovão, SE, Brazil

ARTICLE INFO

Handling Editor: Piotr Ulanski

Keywords:
Radiation detection and measurement
Thermoluminescence
Optically stimulated luminescence
Structure properties
And optical properties

ABSTRACT

This study systematically evaluates the thermoluminescence (TL) and optically stimulated luminescence (OSL) properties of $CaSO_4$ crystals doped with manganese (Mn) and terbium (Tb), focusing on dopant concentrations within the ranges of Mn (0.1 mol % – 2 mol %) and Tb (0.05 mol % – 1 mol %). Synthesized via the slow evaporation route, this investigation is part of an ongoing experimental series initiated by Silva et al. (2022), exploring $CaSO_4$:Mn,Tb crystals at a concentration of 0.1 mol %, validating their properties for dosimetric purposes. A structural phase identification was conducted using X-ray diffraction and energy-dispersive spectroscopy (EDS) spectra confirming the presence of Tb^{3+} and Mn^{2+} ions in the crystalline matrices. Dosimetric characterization utilized pellets prepared by incorporating Teflon into the phosphors. In-depth investigations involved analyzing TL glow curves and Continuous Wave Optically Stimulated Luminescence (CW-OSL) curves. Observations revealed that TL intensity increased as the co-doped concentration of Tb decreased while maintaining the concentration of Mn constant, in both visible and UV regions. Conversely, at a constant terbium concentration, increasing Mn^{2+} concentration enhanced the sensitivity of low-temperature TL traps in the visible region. However, at higher Mn concentrations, such as 1 % and 2 %, TL intensity in deeper traps decreased. In the UV region, TL signals remained stable as the concentration of Mn^{2+} increased from 0.1 % to 0.5 %, with only a slight shift in peak temperatures. Concentrations above 1 % led to a decrease in TL intensity. All samples produced suitable OSL curves. Fixing Mn^{2+} at 1 mol % and decreasing Tb^{3+} concentration also resulted in increased OSL signals. The optimal Mn^{2+} concentration, with Tb^{3+} fixed at 0.1 mol %, was found to be at 0.1 mol %, where OSL sensitivity was maximized. This research underscores the importance of optimizing dopant concentrations to enhance the potential of these phosphors for precise and reliable dosimetry, thereby advancing both the understanding of these materials and their potential for further development in the field of radiation dosimetry.

1. Introduction

Ionic compounds, particularly sulfates, have emerged as prominent host materials for accommodating various luminescent ions, including transition metals and lanthanides, as dopants and co-dopants. Within this array of compounds, calcium sulfate ($CaSO_4$) crystals stand out not only for its luminescent properties but also for its dosimetric applications. Other notable sulfates, such as lithium sulfate (Dhoble et al., 2003; Puppalwar et al., 2011), strontium sulfate (Tang et al., 2006), magnesium sulfate (Upadhyay et al., 2008), sodium sulfate (Gaikwad et al., 2016), and barium strontium sulfate (Aboelezz et al., 2022), have also been investigated for their dosimetric potential.

The choice of dopants plays a crucial role in defining the thermoluminescent (TL) and optically stimulated luminescent (OSL) properties of $CaSO_4$. Among the most commonly used dopants, rare-earth elements such as europium (Eu), thulium (Tm), terbium (Tb), samarium (Sm), and dysprosium (Dy), as well as transition metals like manganese (Mn) and silver (Ag), alkaline earth metals like magnesium (Mg), and alkali metals like lithium (Li), have been widely explored for the their ability to enhance luminescent efficiency and stability. Furthermore, the production of these compounds can be accomplished by diverse methods or synthesis routes, such as the co-precipitation, recrystallization, wet

This article is part of a special issue entitled: ISRP-16 published in Radiation Physics and Chemistry.

* Corresponding author.
E-mail address: andersonmanoel22@hotmail.com (A.M.B. Silva).

https://doi.org/10.1016/j.radphyschem.2025.113032
Received 18 November 2024; Received in revised form 14 April 2025; Accepted 2 June 2025
Available online 3 June 2025

chemistry, solid-state diffusion, roasting-leach, hydrothermal, sol-gel, solid-state reaction, and slow evaporation, as documented in various studies (Bahl et al., 2017; Guckan et al., 2017, 2019, 2023; Junot et al., 2011, 2014, 2016, 2019, 2020, 2024; Kadari et al., 2016; Khan et al., 2015; Kulkarni et al., 2014; Rani et al., 2015; Silva et al., 2020, 2021, 2022, 2023, 2024; Souli et al., 2019; Xu et al., 2019; Yamashita et al., 1970; Zahedifar et al., 2011).

In this work, the choice of dopants, the preparation via slow evaporation route, and the dosimetric characterization of $CaSO_4$:Mn,Tb are based on a continuous study cycle initiated by our research group (Silva et al., 2020, 2021, 2022, 2023, 2024). Our previous experiments revealed promising results for the incorporation of unusual rare-earth elements, such as terbium (Tb), as dopants in $CaSO_4$ matrices. $CaSO_4$:Tb exhibits a TL emission curve with three peaks at 180 °C, 210 °C, and 270 °C, and a TL signal fading of approximately 60 % after 30 days of irradiation (Silva et al., 2020). In the case of $CaSO_4$ monodoped with manganese (Mn), crystal production via the slow evaporation route resulted in a significant reduction in its fading compared to that observed in previous studies using other preparation methods (Bahl et al., 2017; Menon et al., 2005). Furthermore, this compound showed high sensitivity to low doses compared to commercial dosimeters and a fading of 75 % after 30 days (Silva et al., 2023).

Initial studies with a concentration of 0.1 mol % of dopants revealed that the incorporation of Tb as a co-dopant in the $CaSO_4$:Mn matrix results in a TL emission curve with two distinct peaks; the first around 205 °C and the second, more intense, at 325 °C. These analyses indicate the presence of polycrystalline charge trapping centers at energy levels between 0.74 eV and 1.0 eV. Additionally, it was found that the fading of TL emission from co-doped samples was only 16.8 % over a period of 30 days (Silva et al., 2022).

With respect to the OSL signal, we observed a reduction of 49.73 % for $CaSO_4$:Tb and 60.14 % for $CaSO_4$:Mn after 30 days, compared to the OSL signal recorded immediately after irradiation. It is noteworthy that the fading of $CaSO_4$:Mn,Tb was even lower, with a reduction of 9.64 % after the same period of time. This suggests that the co-doping with Mn and Tb resulted in a significant improvement in the stability of the OSL signal compared to samples doped with Tb or Mn alone. This improvement in stability can be attributed to the ability of codoping to generate point structural defects that result in new charge recombination centers located at deeper energy levels. These new recombination centers help reduce the fading of the luminescent signal (Silva et al., 2024).

The characteristic luminescent emissions of the terbium ion, acting as a dopant in the $CaSO_4$ lattice, occur through $4f^8 \rightarrow 4f^8$ transitions, in various wavelength ranges, especially in the visible and ultraviolet spectral regions. On the other hand, in samples doped with manganese only, these emissions are dominant in the green region of the spectrum, around 494 nm, due to the $^4T1\ (^4G) \rightarrow {}^6A_1(^6S)$ transition. The spectral band overlap of Tb^{3+} and Mn^{2+} ions results in more efficient generation of point defects, contributing to the luminescent and dosimetric properties of the $CaSO_4$:Mn,Tb material (Silva et al., 2022).

Although $CaSO_4$:Mn,Tb compounds have been previously investigated for their potential use in radiation dosimetry, a more in-depth understanding of their luminescent emission mechanisms and the role of point defects is essential for their reliable use in routine dosimetry systems. In this work, we investigate the effect of varying the concentration of Mn^{2+} (0.1 mol % - 2 mol %) and Tb^{3+} (0.05 mol % - 1 mol %) dopants on the luminescence properties of $CaSO_4$ crystals. This extends the experimental framework established by Silva et al. (2022, 2024).

To address the current lack of detailed understanding of the influence of dopant concentration, we have systematically evaluated the effects of co-doping on the structural integrity, morphology, and luminescent performance of the compounds. The samples were characterized by X-ray diffraction (XRD), scanning electron microscopy (SEM), and energy-dispersive spectroscopy (EDS). Thermoluminescent glow curves were analyzed in the ultraviolet (UV) and visible (VIS) spectral regions using selective optical filters.

2. Materials and methods

Our methodology employs the slow evaporation method, a well-established technique for sulfate crystal synthesis. For each material, a solution containing calcium carbonate ($CaCO_3$), sulfuric acid (H_2SO_4), terbium oxide (Tb_4O_7), and manganese nitrate ($Mn(NO_3)_2.4H_2O$) was prepared, allowing precise control of the dopant concentrations as we aimed to optimize them for maximal luminescent properties while maintaining structural integrity.

To prepare the crystals, we employ the Yamashita method (Yamashita et al., 1970), characterized by its slow evaporation approach, with specific modifications to enhance crystal growth conditions. These modifications, inspired by the contributions of Junot et al. (2016), include the implementation of a controlled air atmosphere and an improved distillation system that minimizes the risk of external contamination during crystal synthesis, thereby enhancing reliability and reproducibility.

The crystal growth system comprises three key components: a sealed system, an air circulation system, and a heating system, with crystal growth parameters established based on prior studies to ensure optimal conditions. The evaporation temperature is maintained at 375 °C using a heating mantle until the acid is completely evaporated, then the crystals are washed, ground, and sieved. The resulting powders are calcined at 600 °C/1h and are then homogeneously blended with polytetrafluoroethylene (Teflon) to increase material strength. By applying a uniaxial pressure of 0.5 tons, meticulously crafted pellets are produced, followed by sintering to improve strength and stability. The resulting cylindrical pellets have a mass of 30 mg and a diameter of 4 mm. For sintering, the pellets are kept at 400 °C for 1 h and then they are slowly cooled down until they reach a thermal equilibrium with the environment.

XRD patterns were recorded using a Rigaku diffractometer (RINT, 2000/PC) with Cu-Kα radiation, operating at a generator voltage of 60 kV and a current of 30 mA. The analysis was performed in continuous scanning mode over the range of 20°–80° (2θ), with increments of 0.02° per step. The obtained XRD patterns were then compared with reference data from the International Centre for Diffraction Data (ICDD). Size, morphology, and structure of the powder and pellet samples were analyzed using a scanning electron microscope (model JSM-IT700HR) equipped with an EDS system. TL and OSL measurements were conducted using a DA-20 model RisØ TL/OSL reader system, which is equipped with a $^{90}Sr+^{90}Y$ beta source for sample irradiation, providing a dose rate of 4.3368 Gy/min. For signal detection, a bialkaline photomultiplier tube (PMT) was employed, and Schott BG-39 (transmittance in the VIS region between 320 nm and 480 nm). Hoya U340 bandpass filter (transmittance in the UV region between 260 nm and 400 nm) were positioned in front of the PMT to regulate the wavelengths. In TL measurements, a heating rate of 10 °C/s was utilized, with the temperature reaching a maximum of 400 °C. Regarding OSL measurements, the signal acquisition lasted for 40 s, and the samples were stimulated with blue LEDs operating in continuous-wave mode at a wavelength of 470 nm.

3. Results and discussions

3.1. Structural, elemental and morphological characteristics

The effect of different molar ratios of manganese and terbium ions on the structure and morphology of the $CaSO_4$ was first investigated. As shown in Fig. 1, the XRD of the samples exhibited the typical one of the orthorhombic anhydride structures (ICDD 00-037-1496). Strong peaks at 2θ angles of 25.43°, 31.36°, 52.23 and 52.59° are attributed to the (020), (012), (040) and (400) planes, respectively. Additional peaks at 2θ angles of 36.29°, 38.64°, 40.81°, 41.31°, 48.37°, 49.13°, 55.72°, 58.98°,60.66° and 62.23° correspond to the (220), (202), (212), (301), (032), (321), (232), (240), (402), and (412) planes, respectively. The clearly identifiable Bragg peaks indicate the absence of secondary

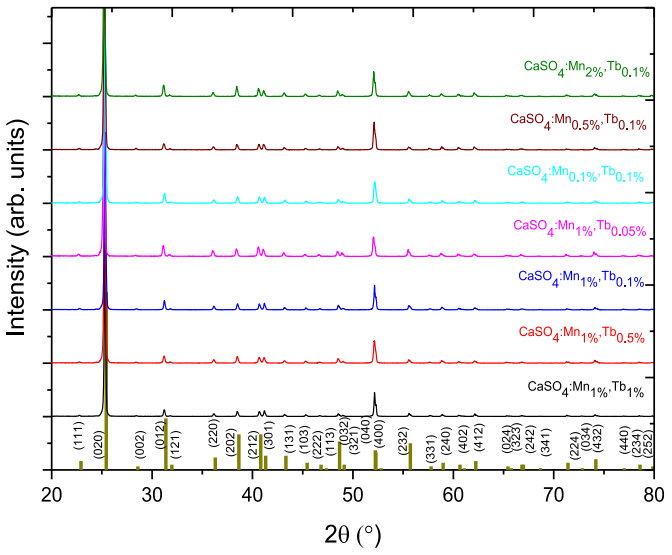

Fig. 1. XRD patterns of $CaSO_4$ samples with different molar ratios of Tb^{3+} and Mn^{2+}.

phases in the samples. Furthermore, the XRD patterns indicate that the overall crystal structure remains stable with the variation of Tb^{3+} and Mn^{2+} concentrations. This suggests effective incorporation of these ions into the Ca^{2+} sites due to their closely matching ionic radii. However, systematic shifts of the diffraction peaks, observed in comparison to the ICDD reference data, suggest subtle lattice distortions. These shifts are likely due to slight variations in ionic radii and to local strain effects from dopant incorporation.

The elemental analysis, performed using energy-dispersive spectroscopy (EDS) on phosphors with varying molar ratios of terbium (Tb^{3+}) and manganese (Mn^{2+}) ($CaSO_4$:$Mn_{0.1\ \%}$,$Tb_{0.1\ \%}$, $CaSO_4$:$Mn_{1\ \%}$, $Tb_{0.1\ \%}$, $CaSO_4$:$Mn_{1.0\ \%}$, $Tb_{0.05\ \%}$, and $CaSO_4$:$Mn_{0.5\ \%}$, $Tb_{0.1\ \%}$) revealed intense peaks for oxygen (O), sulfur (S), and calcium (Ca). These peaks indicate the presence of the initial reactants in the prepared phosphors. Additionally, peaks related to the Tb and Mn ions are also observed in the spectra, despite their low concentrations ($\leq$1 % mol). The atomic percentages of the elements and dopants found are detailed in Fig. 2a. Furthermore, in Fig. 2b, EDS mapping of $CaSO_4$ illustrate the dispersion of Tb and Mn elements, thereby confirming that they are well-distributed on the surface.

The morphological study of the phosphor at 2000 × magnification is shown in Fig. 3a–d. The grains of $CaSO_4$ samples obtained after calcination are agglomerated with a non-uniform shape and have various crystal dimensions. Additionally, the surfaces of the phosphor pellets were analyzed to assess the grain behavior after pressing and sintering (Fig. 3e–f). Fig. 3e shows that $CaSO_4$:Mn,Tb pellets with Teflon have a homogeneous and cohesive surface. At higher magnification (2200 ×), small Teflon agglomerates can be seen on the surface of the pellet in Fig. 3f, highlighting the low porosity of the pellets. This low porosity is essential for dosimetric applications as it enhances thermal conductivity in the pellets, blocks moisture and contaminants, and ensures uniform radiation absorption. These features help preserve the consistency of the emitted luminescence signal and prevent grain breakage and detachment.

3.2. *Effect of impurity concentration on TL/OSL properties of $CaSO_4$:Mn,Tb*

To investigate the effect of dopant concentrations of Tb^{3+} and Mn^{2+} on the luminescence curves of $CaSO_4$:Mn,Tb samples and to pinpoint the optimal dopant concentration that results in the highest luminescence sensitivity, TL and OSL signals were recorded using pellet samples. The study of impurity concentration variation began by fixing the Mn^{2+} ion concentration at 1 mol % and then varying the Tb^{3+} ion concentrations from 0.05 mol % to 1 mol %. Then, keeping terbium concentration constant at 0.1 %, Mn^{2+} concentration was increased from 0.1 % to 2 %. The overall TL properties of the samples were analyzed both in the visible and in the UV range. By using Schott BG39 (Fig. 4a) and Hoya U340 (Fig. 4b) filters and varying the concentration of Tb^{3+}, we observed an increase in TL signals in both the visible and UV regions as the concentration of Tb^{3+} decreased. This suggests a correlation between Tb^{3+} concentration and TL intensity. As the concentration of Tb^{3+} decreases, we observed an increase in TL response in the low-temperature region, while a decrease was also noted in the deep trap region. Another observation is that only at concentrations below 0.5 mol % of Tb^{3+} is the intensity in the shallow trap region in the visible range higher than that of the TL traps in the high-temperature region, while in the UV regions this is observed at concentrations below 0.1 mol %.

On the other hand, in the visible region, TL signals showed an increase in sensitivity of the low-temperature trap with increasing concentrations of Mn^{2+}, while keeping the Tb^{3+} concentration fixed at 0.1 %. However, for the Mn concentrations of 1 mol % and 2 mol %, a reduction in the TL intensity was observed in the deeper traps (see Fig. 5a).

In the UV region, as shown by the TL signals in Fig. 5b, the behavior of TL signals varies significantly with changes in Mn^{2+} concentration. First, it is observed that increasing the Mn^{2+} concentration results in a greater number of deeper traps. This behavior indicates that Mn plays a

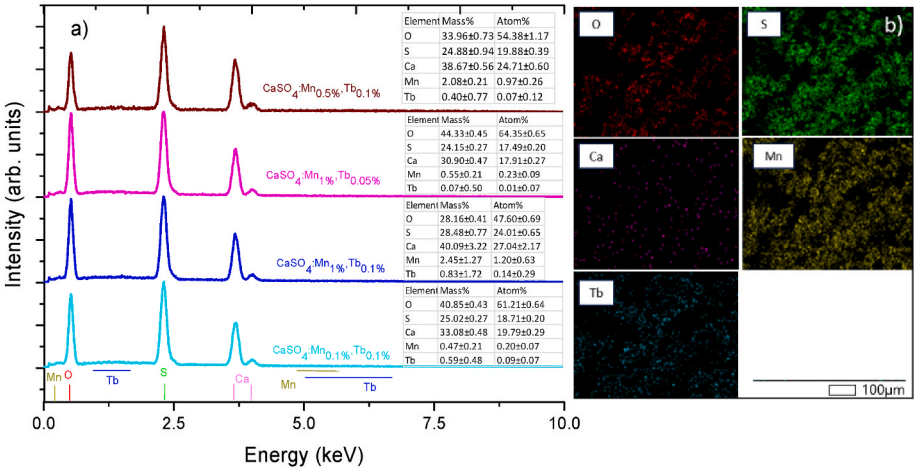

Fig. 2. a) EDS spectra of $CaSO_4$ samples with varying molar ratios of Tb^{3+} and Mn^{2+} and b) EDS mapping results of $CaSO_4$:$Mn_{1\ \%}$,$Tb_{0.05\ \%}$; scale bar 100 μm.

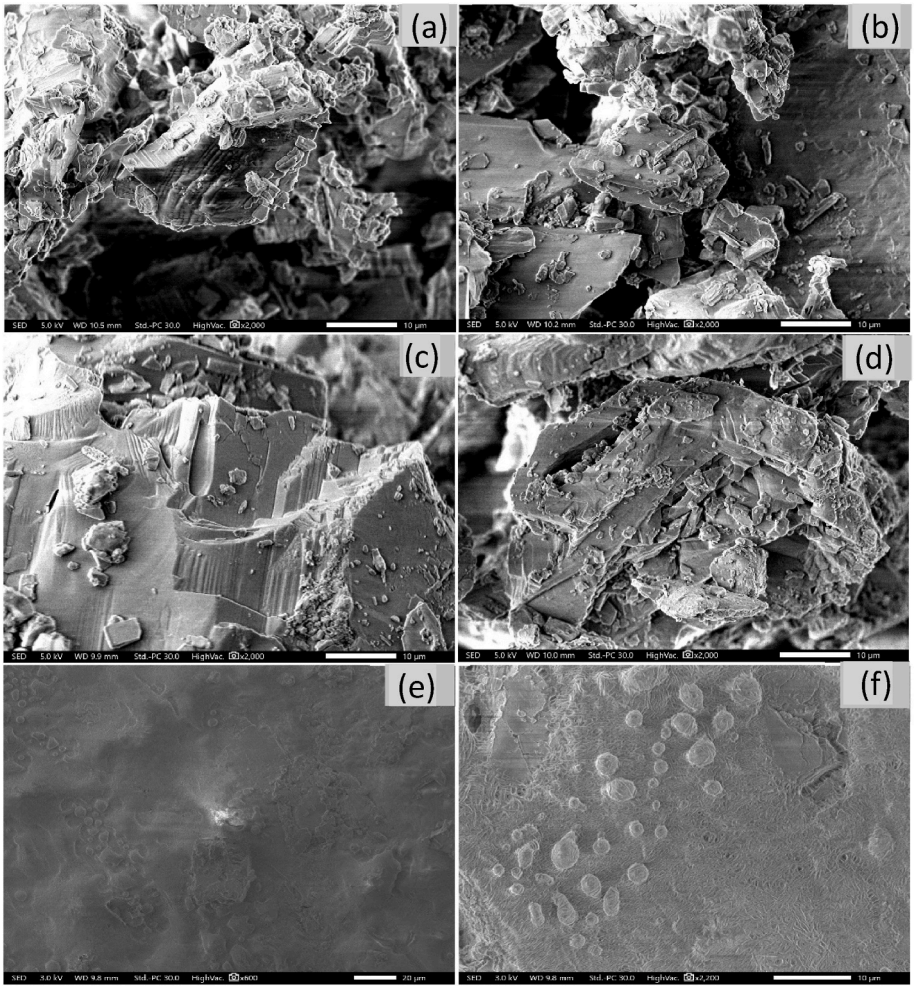

Fig. 3. (a–d) SEM micrographs of $CaSO_4$ powders: (a) $CaSO_4$:$Mn_{0.1\ \%}$, $Tb_{0.1\ \%}$; (b) $CaSO_4$:$Mn_{1\ \%}$,$Tb_{0.1\ \%}$;(c) $CaSO_4$:$Mn_{1\ \%}$,$Tb_{0.05\ \%}$; (d) $CaSO_4$:$Mn_{0.5\ \%}$,$Tb_{0.1\ \%}$. (e–f) SEM images of phosphorus pellets at different magnifications, illustrating the grain behavior after pressing and sintering.

beneficial role in boosting the efficiency of these traps, as deeper traps are able to store electrical charge for a long time. Electrons trapped in these deeper locations require more energy to release, which diminishes the likelihood of unintentional recombination and consequent loss of dosimetric information.

The impurity concentration of 1 mol % of Mn resulted in a comparatively more intense TL peak, indicating that this concentration is optimal for maximizing the luminescent centers. However, increasing the Mn concentration from 0.1 % mol to 0.5 % mol and beyond (1 mol % and 2 mol %) leads to a decrease in TL intensity. This phenomenon is due to the decrease in distance between the active ions resulting from the increase in dopant concentration. As the ions approach each other, they tend to interact with each other, resulting in a loss of TL signal intensity. Higher dopant concentration may lead to non-radiative transitions or in transitions that do not fall within the spectral response of the PMT (Sen et al., 2024). This nuanced understanding of the role of Mn as a dopant highlights the delicate balance required to optimize its concentration with the intent to enhance the dosimetric properties of the host material. These results complement and extend the conclusions of previous studies (Silva et al., 2022, 2024), in which the co-doped sample (0.1 mol % Mn^{2+}, 0.1 mol % Tb^{3+}) showed a strong potential for TL and OSL dosimetry under Hoya optical filter conditions. At this concentration, the material exhibited a well-defined OSL decay curve, a TL glow curve with two prominent peaks at 205 °C and 325 °C, good signal reproducibility, and linear dose-response. Silva et al. (2024) also compared co-doped samples with mono-doped ones and confirmed a superior dosimetric performance of the former, mainly due to their significantly reduced fading.

In the context of OSL dosimetry, the effects of different dopant concentrations on the OSL decay curves were investigated. Fig. 6 illustrates the OSL curves of samples irradiated with 1 Gy, obtained in continuous mode (CW) with a 40 s integration time. These curves are plotted on a semi-log scale to help clarity. It is observed that all samples exhibit a characteristic exponential decay, indicating that the traps are being emptied during optical stimulation. Fixing Mn^{2+} at 1 mol % and decreasing the Tb^{3+} concentration also resulted in increased OSL signals (see Fig. 6a). The optimal Mn^{2+} concentration, with Tb^{3+} fixed at 0.1 mol %, was achieved at 0.1 mol % of Tb^{3+}, where OSL sensitivity was maximized. Concentrations above 0.1 mol % of Mn^{2+} did not enhance OSL performance of the pellets (Fig. 6b).

Fig. 7a and (b) present the TL glow curves of $CaSO_4$:Mn,Tb samples with the highest TL intensities ($CaSO_4$:$Mn_{1\ \%}$,$Tb_{0.05\ \%}$, $CaSO_4$:$Mn_{1\ \%}$, $Tb_{0.1\ \%}$, $CaSO_4$:$Mn_{0.5\ \%}$,$Tb_{0.1\ \%}$, and $CaSO_4$:$Mn_{0.1\ \%}$,$Tb_{0.1\ \%}$) measured using Schott BG39 and Hoya U340 optical filters, respectively. Despite slight variations in intensity and peak positions, the glow curve shapes remain consistent across all samples and filters. This confirms that the TL behavior is intrinsic to the material and stable across both UV and visible regions, reinforcing its suitability for reliable dosimetric applications.

A particularly notable observation is that the TL signals recorded with the Hoya U340 filter (Fig. 7b) show significantly higher intensity in the high-temperature region compared to those measured with the

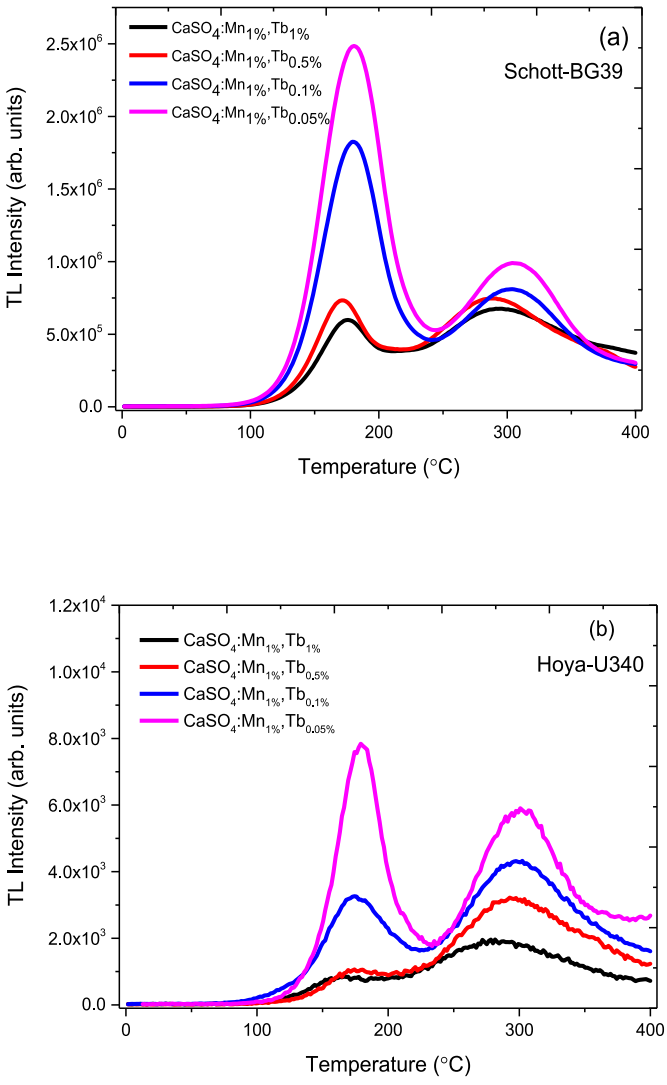

Fig. 4. TL emission curves of $CaSO_4$:Mn,Tb samples irradiated with 1 Gy of beta radiation, obtained using (a) Schott BG39 and (b) Hoya U340 filters in the TL reader. Concentration quenching study started with 1 mol % Mn^{2+} ion concentration, varying Tb^{3+} ion concentrations from 0.05 % to 1 mol %.

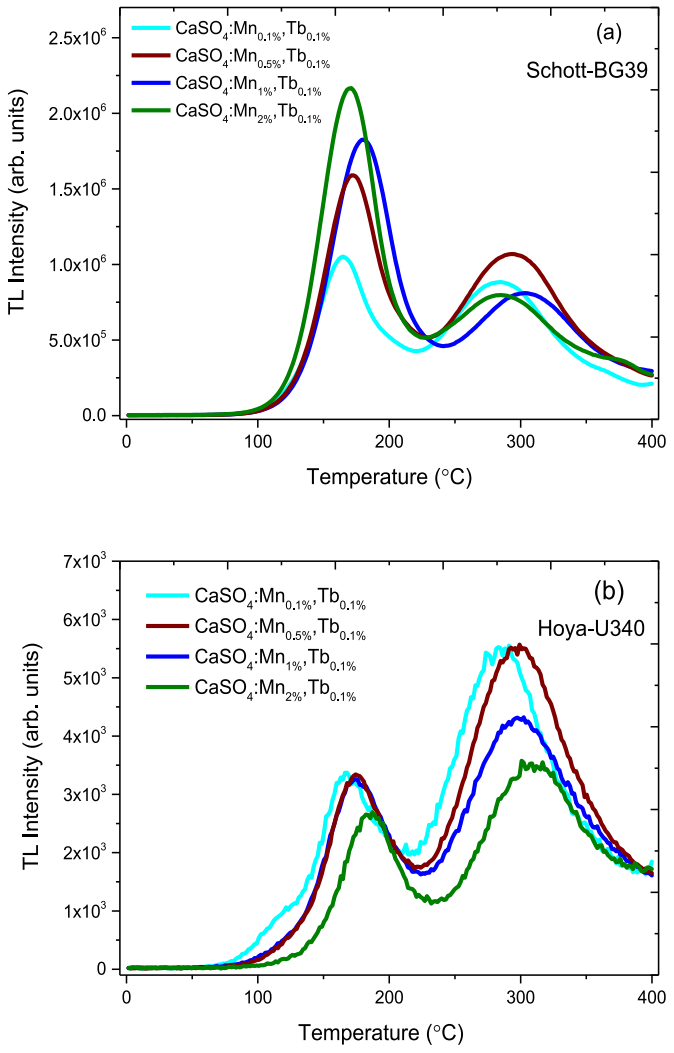

Fig. 5. TL emission curves of $CaSO_4$:Mn,Tb irradiated with 1 Gy of beta radiation, obtained using samples under (a) Schott BG39 and (b) Hoya U340 filters. Terbium concentration was held constant at 0.1 %, while Mn^{2+} ion concentrations were varied from 0.1 % to 2 mol %.

Schott BG39 filter (Fig. 7a). This high-temperature peak is especially advantageous for dosimetric applications, as it is due to a higher concentration of charge carriers trapped in deeper energy levels. These deeper traps contribute to an improved signal stability by reducing the release of thermally unstable carriers, thereby improving the accuracy and reliability of TL/OSL dosimetry.

Fig. 8 presents the integrated TL signal obtained by calculating the area under each emission curve. The results clearly demonstrate the significant influence of dopant concentration on luminescence efficiency.

Similarly, OSL decay curves for the samples with optimized dopant concentrations were recorded and compared under Hoya U340 filters (Fig. 9). In particular, the sample doped with 0.05 mol % Tb^{3+} exhibited the highest TL/OSL intensity, suggesting that the optimal doping concentrations for $CaSO_4$:Mn,Tb are 0.05 mol % Tb^{3+} and 1 mol % Mn^{2+}, following calcination at 600 °C.

4. Conclusions

In this study, different concentrations of Tb^{3+} and Mn^{2+}doped $CaSO_4$ samples were successfully synthesized by a slow evaporation method. XRD patterns indicated that the crystal structure and phase of $CaSO_4$ remained unchanged with the addition of Mn^{2+} and Tb^{3+} ions. Scanning electron microscopy images of $CaSO_4$ powders and pellets revealed agglomerated, non-uniform grains in the phosphor powder, and a cohesive, low-porosity surface in the pressed pellets, which is crucial for enhancing thermal conductivity and ensuring consistent luminescence in dosimetric applications. EDS spectra confirmed the presence of O, S, and Ca as major constituents in the prepared $CaSO_4$ phosphors, along with well-distributed Tb^{3+} and Mn^{2+} dopants, indicating successful incorporation of the dopants into the crystal lattice.

Intending to use phosphors for dosimetric applications, the luminescence properties of the samples were comprehensively compared based on their response to beta radiation. These analyses showed that the TL intensity of $CaSO_4$:Mn,Tb depends on the concentrations of Tb^{3+} and Mn^{2+}. The TL peak heights were more significantly influenced by the Tb^{3+} concentration. For a constant Mn^{2+} concentration, the TL intensity increased as the concentration of co-doped Tb^{3+} decreased, both in the visible and in the UV regions. Mn concentrations of higher than 0.1 mol % do not contribute significantly to the maximum peak height and TL intensity in the UV region. In the visible region, increasing Mn^{2+} concentrations while keeping Tb^{3+} at a fixed level of 0.1 mol % enhanced the intensity of the low-temperature TL traps. However, at Mn^{2+} concentrations of 1 mol % and 2 mol %, the TL intensity in deeper

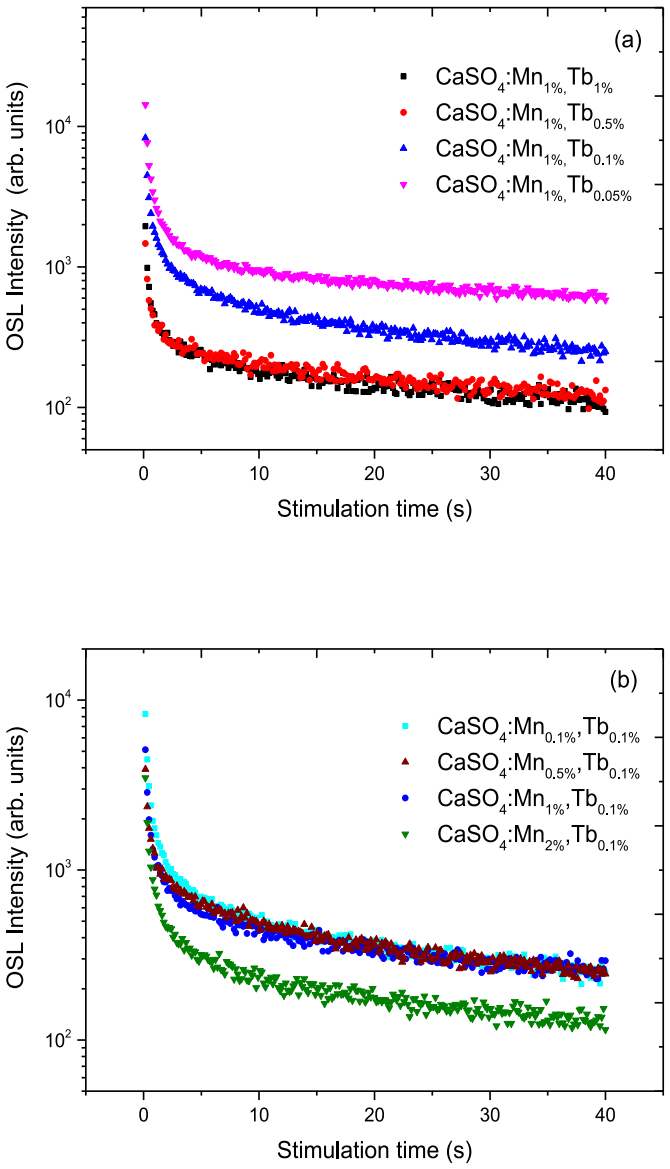

Fig. 6. The change in OSL signals of (a) $CaSO_4$:$Mn_{1\ \%}$,Tb_x (x = 1, 0.5, 0.1, 0.05) pellets and (b) $CaSO_4$:Mn_x,$Tb_{0.1\ \%}$ (x = 0.1, 0.5, 1, 2) pellets.

traps decreased. A comparison of the OSL curves for different concentrations of Tb^{3+} and Mn^{2+} revealed that the pellets also exhibited a potential dosimetric performance by this technique. The optimal Mn^{2+} concentration, with Tb^{3+} fixed at 0.1 mol %, was found to be 0.1 mol %, at which point OSL sensitivity was maximized. Concentrations exceeding 0.1 mol % of Mn^2 did not enhance OSL performance. We concluded that the optimal concentrations of Tb^{3+} and Mn^{2+} dopants are 0.05 mol % and 1 mol %, respectively, following calcination at 600 °C.

CRediT authorship contribution statement

A.M.B. Silva: Writing – review & editing, Writing – original draft, Methodology, Investigation, Formal analysis, Data curation, Conceptualization. **D.N. Souza:** Funding acquisition, Project administration, Supervision, Validation, Visualization. **L.V.E. Caldas:** Funding acquisition, Project administration, Supervision, Visualization.

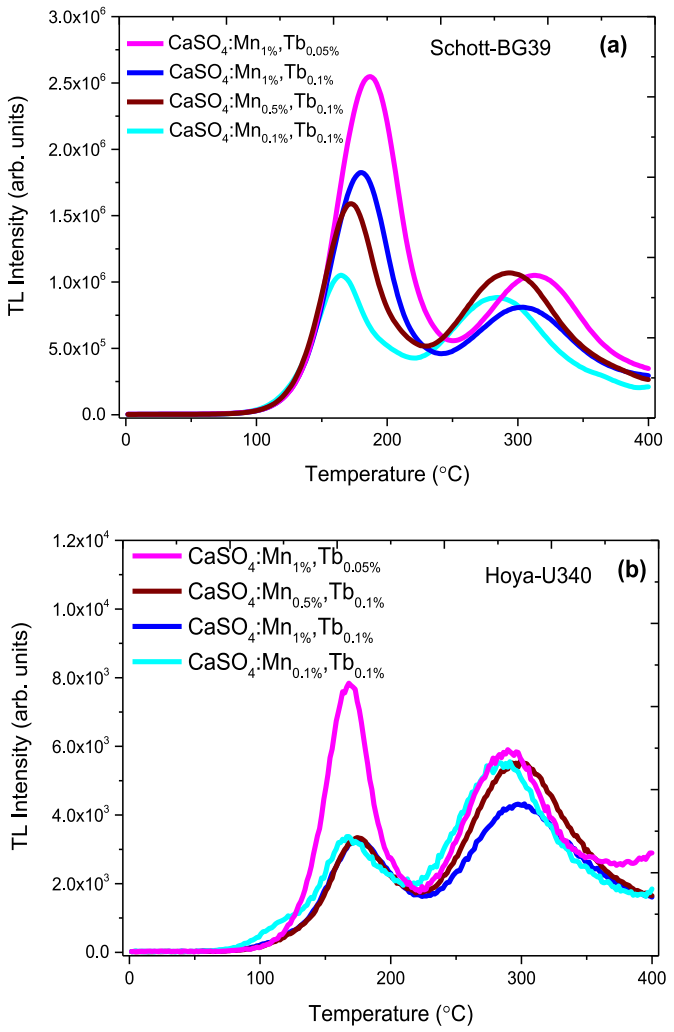

Fig. 7. TL emission curves of pellets with optimized Tb and Mn concentrations ($CaSO_4$:$Mn_{1\ \%}$,$Tb_{0.05\ \%}$, $CaSO_4$:$Mn_{1\ \%}$, $Tb_{0.1\ \%}$, $CaSO_4$:$Mn_{0.5\ \%}$, $Tb_{0.1\ \%}$, and $CaSO_4$:$Mn_{0.1\ \%}$, $Tb_{0.1\ \%}$), irradiated with 1 Gy of beta radiation, obtained using (a) Schott BG39 and (b) Hoya U340 filters.

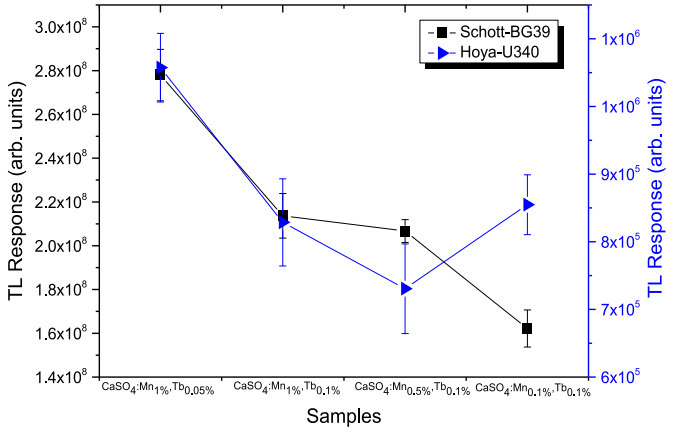

Fig. 8. TL signal obtained by integrating the area under the glow curves of $CaSO_4$:Mn,Tb samples with different dopant concentrations: $CaSO_4$:$Mn_{1\ \%}$, $Tb_{0.05\ \%}$, $CaSO_4$:$Mn_{1\ \%}$, $Tb_{0.1\ \%}$, $CaSO_4$:$Mn_{0.5\ \%}$, $Tb_{0.1\ \%}$, and $CaSO_4$:$Mn_{0.1\ \%}$, $Tb_{0.1\ \%}$.

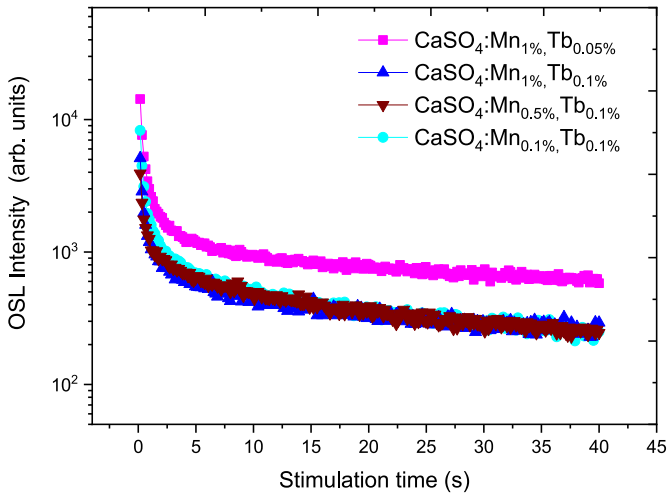

Fig. 9. OSL decay curves for samples with optimized dopant concentrations ($CaSO_4$:$Mn_{1\ \%}$,$Tb_{0.05\ \%}$, $CaSO_4$:$Mn_{1\ \%}$, $Tb_{0.1\ \%}$, $CaSO_4$:$Mn_{0.5\ \%}$, $Tb_{0.1\ \%}$, and $CaSO_4$:$Mn_{0.1\ \%}$, $Tb_{0.1\ \%}$), irradiated with 1 Gy of beta radiation, analyzed under Hoya U340 filter.

Declaration of competing interest

The authors declare the following financial interests/personal relationships which may be considered as potential competing interests: Anderson Manoel Bezerra da Silva reports financial support was provided by State of Sao Paulo Research Foundation. Linda Viola Ehlin Caldas reports financial support was provided by State of Sao Paulo Research Foundation. Divanizia do Nascimento Souza reports was provided by National Council for Scientific and Technological Development. Reports a relationship with that includes:. Has patent pending to. If there are other authors, they declare that they have no known competing financial interests or personal relationships that could have appeared to influence the work reported in this paper.

Acknowledgments

The authors gratefully acknowledge the support of the Brazilian agencies: Fundação de Amparo à Pesquisa do Estado de São Paulo (FAPESP, Projects: 2023/04859–8 and 2018/05982–0); Conselho Nacional de Desenvolvimento Científico e Tecnológico (CNPq, Projects: 305142/2021–6, 07493/2021–2, 405536/2023–2, and 406761/2022–1); and Comissão Nacional de Energia Nuclear (CNEN, Project: 1342.005453/2023–19).

Data availability

Data will be made available on request.

References

Aboelezz, E., Bortolin, E., Quattrini, M.C., Della, Monaca S., 2022. TL and OSL studies on irradiated nano barium strontium sulfate to photons, electrons and protons. J. Lumin. 242, 118592. https://doi.org/10.1016/j.jlumin.2021.118592.

Bahl, S., Kumar, V., Bihari, R.R., Kumar, P., 2017. Investigations of OSL properties of $CaSO_4$:Mn phosphor exposed to gamma and beta radiations. J. Lumin. 181, 36–43. https://doi.org/10.1016/j.jlumin.2016.09.004.

Dhoble, S.J., Shahare, D.I., Moharil, S.V., 2003. Synthesis and characterization of Li_2SO_4: P,RE (RE=Dy or Eu), low Z, TLD phosphors. Phys. Status Solidi, A Appl. Res. 198, 183. https://doi.org/10.1002/pssa.200306591.

Gaikwad, S.U., Patil, R.R., Kulkarni, M.S., Bhatt, B.C., Moharil, S.V., 2016. Thermoluminescence and optically stimulated luminescence in various phases of doped Na_2SO_4. Phase Transitions 89, 202–210. https://doi.org/10.1080/01411594.2015.1065494.

Guckan, V., Altunal, V., Nur, N., Depci, T., Ozdemir, A., Kurt, K., Yu, Y., Yegingil, I., Yegingil, Z., 2017. Studying $CaSO_4$:Eu as an OSL phosphor. Nucl. Instrum. Meth. Phys. Res. B: Beam Interact. Mater. At. 407, 145–154. https://doi.org/10.1016/j.nimb.2017.06.010.

Guckan, V., Bereket, S., Altunal, V., Abusaid, W., Yegingil, Z., 2023. Luminescence properties of Tb and Eu activated $CaSO_4$ phosphor. Radiat. Phys. Chem. 203, 110620.

Guckan, V., Ozdemir, A., Altunal, V., Yegingil, I., Yegingil, Z., 2019. Studies of blue light induced phototransferred thermoluminescence in $CaSO_4$:Mg. Nucl. Instrum. Methods Phys. Res. B 448, 31–38.

Junot, D.O., Galeano, D.C., Silva, A.M.B., Souza, D.N., Caldas, L.V.E., 2024. Development of $CaSO_4$:RE,Li (RE= Tm, Eu, Tb) composites for thermally or optically stimulated luminescence dosimetry. Radiat. Meas., 107217

Junot, D.O., Santos, A.G., Antonio, P.L., Rezende, M.V., Souza, D.N., Caldas, L.V.E., 2019. Dosimetric and optical properties of $CaSO_4$:Tm and $CaSO_4$: Tm, Ag crystals produced by a slow evaporation route. J. Lumin. 210, 58–65. https://doi.org/10.1016/j.jlumin.2019.02.005.

Junot, D.O., Souza, D.N., Caldas, L.V.E., 2020. TL/OSL signal of $CaSO_4$: Eu, Ag samples produced by variations of the slow evaporation route. Radiat. Meas. 135, 106334. https://doi.org/10.1016/j.radmeas.2020.106334.

Junot, D.O., Barros, J.P., Caldas, L.V.E., Souza, D.N., 2016. Thermoluminescent analysis of $CaSO_4$:Tb,Eu crystal powder for dosimetric purposes. Radiat. Meas. 90, 228–232. https://doi.org/10.1016/j.radmeas.2016.01.020.

Junot, D.O., Santos, M.A.C., Antonio, P.L., Caldas, L.V.E., Souza, D.N., 2014. Feasibility study of $CaSO_4$:Eu, $CaSO_4$:Eu,Ag and $CaSO_4$:Eu,Ag(NP) as thermoluminescent dosimeters. Radiat. Meas. 71, 99–103. https://doi.org/10.1016/j.radmeas.2014.05.022.

Junot, D.O., Vasconcelos, D.F., Chagas, M.A.P., Santos, M.A.C., Caldas, L.V.E., Souza, D.N., 2011. Silver addition in $CaSO_4$:Eu, TL and TSEE properties. Radiat. Meas. 46, 1500–1502. https://doi.org/10.1016/j.radmeas.2011.06.049.

Kadari, A., Mahi, K., Mostefa, R., Badaoui, M., Mameche, A., Kadri, D., 2016. Optical and structural properties of Mn doped $CaSO_4$ powders synthesized by sol-gel process. J. Alloys Compd. 688, 32–36. https://doi.org/10.1016/j.jallcom.2016.07.040.

Khan, Z.S., Ingale, N.B., Omanwar, S.K., 2015. Thermoluminescence studies of terbium doped calcium sulfate phosphor. Int. J. Lumin. Appl. 5, 471–474.

Kulkarni, M.S., Patil, R.R., Patle, A., Rawat, N.S., Ratna, P., Bhatt, B.C., Moharil, S.V., 2014. Optically stimulated luminescence from $CaSO_4$: Eu–Preliminary results. Radiat. Meas. 71, 95–98.

Menon, S.N., Sanaye, S.S., Dhabekar, B.S., Kumar, R., Bhatt, B.C., 2005. Role of Mn as a co-dopant in $CaSO_4$:Mn,Pr TL phosphor. Radiat. Meas. 39, 111–114. https://doi.org/10.1016/j.radmeas.2004.06.004.

Puppalwar, S.P., Dhoble, S.J., Kumar, A., 2011. Improvement of photoluminescence of Cu+ ion in Li_2SO_4. Luminescence (Chichester, Engl.) 26, 456–461. https://doi.org/10.1002/bio.1252.

Rani, R.S., Lakshmanan, A.R., Sivakumar, V., Venkatasamy, R., Annalakshmi, O., Jose, M.T., Marimuthu, K.N., 2015. Redox and charge transfer processes and luminescence in $CaSO_4$:Zn,Mn. Radiat. Meas. 76, 1350–4487. https://doi.org/10.1016/j.radmeas.2015.03.001.

Sen, D., Bahl, S., Seth, P., Singh, B., Pandey, A., Zulfequar, M., Kandasami, A., 2024. Effect of helium ion and gamma irradiation on the TL and OSL properties of Tb-doped LiF nanophosphors. J. Lumin. 271, 120587. https://doi.org/10.1016/j.jlumin.2024.120587.

Silva, A.M.B., Souza, L.F., Antonio, P.L., Junot, D.O., Caldas, L.V.E., Souza, D.N., 2022. Effects of manganese and terbium on the dosimetric properties of $CaSO_4$. Radiat. Phys. Chem. 198, 110207. https://doi.org/10.1016/j.radphyschem.2022.110207.

Silva, A.M.B., Junot, D.O., Caldas, L.V.E., Souza, D.N., 2020. Structural, optical and dosimetric characterization of $CaSO_4$:Tb, $CaSO_4$:Tb,Ag and $CaSO_4$:Tb,Ag(NP). J. Lumin. 224, 117286. https://doi.org/10.1016/j.jlumin.2020.117286.

Silva, A.M.B., Rodrigues, D.S., Antonio, P.L., Junot, D.O., Caldas, L.V.E., Souza, D.N., 2023. Investigation of dosimetric properties of $CaSO_4$:Mn phosphor prepared using slow evaporation route. Appl. Radiat. Isot. 199, 110874. https://doi.org/10.1016/j.apradiso.2023.110874.

Silva, A.M.B., Silveira, W.S., Matos, T.S., Junot, D.O., Rezende, M.V., Souza, D.N., 2021. Effect of terbium and silver co-doping on the enhancement of photoluminescence in $CaSO_4$ phosphors. Opt. Mater. 111, 110717. https://doi.org/10.1016/j.optmat.2020.110717.

Silva, A.M.B., Rodrigues, D.S., Guedes, B.D., Silveira, I.S., Antonio, P.L., Junot, D.O., Caldas, L.V.E., Souza, D.N., 2024. Exploring the luminescence properties and dosimetric characteristics of $CaSO_4$:Tb, $CaSO_4$: Mn, and $CaSO_4$:Mn, Tb phosphors synthesized by slow evaporation route. Radiat. Meas. 177, 107261. https://doi.org/10.1016/j.radmeas.2024.107261.

Souli, M., Reghima, M., Secu, M., Bartha, C., Enculescu, M., Mejri, A., Kamoun-Turki, N., Badica, P., 2019. Physical properties investigation of samarium doped calcium sulfate thin films under high gamma irradiations for space photovoltaic and dosimetric applications. Superlattice. Microst. https://doi.org/10.1016/j.spmi.2018.12.021.

Tang, Q., Zhang, C.X., Luo, D.L., Leung, P.L., Xiong, Z.Y., 2006. TL and OSL of $SrSO_4$ phosphors doped with Eu. Radiat. Protect. Dosim. 119, 238–243. https://doi.org/10.1093/rpd/nci578.

Upadhyay, A., Dhoble, S.J., Rai, R., Kher, R.S., 2008. Synthesis of $KNaSO_4$: Tb^{3+} and $MgSO_4$: Dy^{3+} phosphors for lyoluminescence dosimetry. Nucl. Instrum. Methods Phys. Res. B. 266, 2594–2598. https://doi.org/10.1016/j.nimb.2008.03.236.

Xu, X., Liu, W., Chu, G., Zhang, G., Luo, D., Yue, H., Liang, B., Li, C., 2019. Energy-efficient mineral carbonation of $CaSO_4$ derived from wollastonite via a roasting-

leaching route. Hydro 184, 151–161. https://doi.org/10.1016/j.hydromet.2019.01.004.

Yamashita, T., Sakai, K., Kitamura, S., 1970. Calcium sulfate activated by lead and manganese for thermoluminescence dosimetry. J. Nucl. Sci. (Seoul) 7, 105–110. https://doi.org/10.1080/18811248.1970.9734651.

Zahedifar, M., Mehrabi, M., Harooni, S., 2011. Synthesis of $CaSO_4$:Mn nanosheets with high thermoluminescence sensitivity. Appl. Radiat. Isot. 69, 1002–1006. https://doi.org/10.1016/j.apradiso.2011.01.036.